Research Article | Vol. 29, No. 1 / 4 January 2021 / Optics Express 454

Optics EXPRESS

Switching between singular points in non-*PT*-symmetric multilayer structures using phase-change materials

YIN HUANG,[1,5] LANYAN WANG,[1] YUECHENG SHEN,[2,6] AND GEORGIOS VERONIS[3,4]

[1]*Department of Optoelectrics Information Science and Engineering, School of Physics and Electronics, Central South University, Changsha, Hunan 410012, China*
[2]*State Key Laboratory of Optoelectronic Materials and Technologies, School of Electronics and Information Technology, Sun Yat-Sen University, Guangzhou, Guangdong 510275, China*
[3]*School of Electrical Engineering and Computer Science, Louisiana State University, Baton Rouge, LA 70803, USA*
[4]*Center for Computation and Technology, Louisiana State University, Baton Rouge, LA 70803, USA*
[5]*yhuan15@csu.edu.cn*
[6]*shenyuecheng@mail.sysu.edu.cn*

Abstract: We investigate the switching between singular points in non-parity-time-symmetric multilayer structures using phase-change materials at the optical communication wavelength. We first show that absorbing singularities can be switched to exceptional points (EPs) in a two-layer structure consisting of a phase-change material layer and a lossy layer by switching the phase-change material $Ge_2Sb_2Te_5$ (GST) from its crystalline to its amorphous phase. We also show that spectral singularities (SSs) can be switched to EPs in a three-layer structure consisting of a lossless dielectric layer sandwiched between a GST layer and a gain layer by switching the GST from its crystalline to its amorphous phase. We then show that self-dual SSs can be switched to unidirectional spectral singularities in a three-layer structure consisting of a lossy layer sandwiched between a GST layer and a gain layer by switching the GST from its amorphous to its crystalline phase. In addition, at the unidirectional spectral singularity, zero reflection from one side and infinite reflection from the opposite side are simultaneously realized. We finally show that we can design an active device with large modulation depth achieved by a very small variation of the imaginary part of the refractive index of the active absorbing material in the lossy layer. Our results could potentially contribute to the development of a new generation of singularity-enhanced switchable optical devices.

1. Introduction

Exceptional points (EPs) are singular points in the spectra of non-Hermitian Hamiltonians in open quantum systems that correspond to the coalescence of the eigenvalues and their corresponding eigenvectors [1,2]. Recently, Lin *et al*. demonstrated unidirectional reflectionless light propagation at EPs in non-Hermitian parity-time (*PT*) symmetric optical systems with balanced gain and loss, where the reflection is zero when measured from one side of the structure and nonzero when measured from the other side [3]. Unidirectional reflectionless propagation of light demonstrates the existence of EPs in non-Hermitian optical systems [3–8]. Another type of singular points are spectral singularities (SSs) associated with the lack of completeness of the eigenvectors of non-Hermitian Hamiltonians in the continuous spectra [9,10]. Mostafazadeh showed that optical SSs are zero-width resonances that corresponds to lasing at threshold gain [11]. The reflection and transmission of non-Hermitian optical systems at SSs tend to infinity [11–13]. In addition, coherent perfect absorption (CPA) can be viewed as a time-reversed lasing

#411742 https://doi.org/10.1364/OE.411742
Journal © 2021 Received 6 Oct 2020; revised 10 Dec 2020; accepted 13 Dec 2020; published 24 Dec 2020

Optics EXPRESS

process [14,15], and therefore the CPA point is often referred to as time-reversed SS [10,16]. In particular, a *PT*-symmetric optical system can support a self-dual SS, at which the system can simultaneously act as a laser and a coherent perfect absorber at the same wavelength (CPA-lasing) [15,17–20]. Another type of singular points are unidirectional spectral singularities at which zero reflection from one side and infinite reflection from the opposite side are simultaneously realized [21]. EPs and self-dual SSs can also emerge in non-*PT*-symmetric configurations with unbalanced gain and loss [7,8,16,22]. This is due to the fact that EPs and SSs exist in a larger family of non-Hermitian Hamiltonians [7,16]. Such non-*PT*-symmetric structures are of interest because they can relax the strict requirement of having balanced gain and loss. Singular-point-based optical devices are important for several key applications in photonics, including optical network analyzers [4], switches [22], wave-based information processing [23], perfect absorbers [24], and sensors [25–29]. Implementing multiple types of singular points in a single reconfigurable non-*PT*-symmetric structure could be essential for developing compact optoelectronic devices and highly tunable optical systems. However, switching between different types of singular points in nanophotonic structures has not been investigated before. One of the most promising approaches to achieve this is through the use of phase-change materials.

$Ge_2Sb_2Te_5$ (GST) is a phase-change material with amorphous and crystalline phases [30]. The atom distribution of GST is chaotic in the amorphous phase, while the atoms are aligned in an orderly manner in the crystalline phase. Thus, GST can lead to a drastic change in electrical and optical properties through the transition between the amorphous and crystalline phases. The phase transition can be induced reversibly and rapidly by applying external electrical pulses, optical pulses or thermal annealing. The transition speed can be at subpicosecond timescales via femtosecond laser pulses [31,32]. In addition, power is consumed only during the phase transition process, and no external excitations are required for GST to retain its phase due to its nonvolatility. GST is currently widely used in a variety of reconfigurable optical devices, including memories [32], optical switches [33–35], active displays [36,37], and neural computing technologies [38].

We previously showed that for a three-layer structure, consisting of a gain medium layer sandwiched between two GST layers, unidirectional reflectionlessness in the forward direction can be switched to unidirectional reflectionlessness in the backward direction by switching GST from its amorphous to its crystalline phase [34]. In this paper, we investigate the switching between different types of singular points in non-*PT*-symmetric multilayer structures at the optical communication wavelength using phase-change materials. We first show that switching between coherent perfect absorption and unidirectional reflectionlessness can be achieved in a two-layer structure, consisting of a phase-change material layer and a lossy layer, by switching the phase-change material GST between its crystalline and amorphous phases. In other words, absorbing singularities can be switched to EPs. We also show that switching between lasing and unidirectional reflectionlessness can be realized in a three-layer structure, consisting of a lossless dielectric layer sandwiched between a phase-change material layer and a gain layer, by switching the phase-change material GST between its crystalline and amorphous phases. In other words, SSs can be switched to EPs. We then show that switching between CPA-lasing and left reflectionless-right lasing [21] can be realized in a three-layer structure, consisting of a lossy layer sandwiched between a phase-change material layer and a gain layer, by switching the phase-change material GST between its amorphous and crystalline phases. In other words, self-dual SSs can be switched to unidirectional spectral singularities. In particular, at this unidirectional spectral singularity, zero reflection from one side and infinite reflection from the opposite side are simultaneously realized. This unidirectional spectral singularity is associated with strong resonance trapping in the proposed non-*PT*-symmetric structure. This singularity results in extremely high sensitivity of the reflected light intensity to variations of the imaginary part of the refractive index of the active absorbing material in the lossy layer. We finally show

Optics EXPRESS

that we can design a singularity-enhanced active device with large modulation depth achieved by a very small variation of the imaginary part of the refractive index of the active absorbing material.

The remainder of the paper is organized as follows. In Section 2, we employ the transfer matrix method to account for the behavior of the proposed non-PT-symmetric multilayer structure. In Subsection 3.1 we design a two-layer structure, consisting of a GST layer and a lossy layer, to realize switching between absorbing singularities and EPs. In Subsection 3.2 we design a three-layer structure, consisting of a lossless dielectric layer sandwiched between a GST layer and a gain layer, to realize switching between SSs and EPs. In Subsection 3.3 we use a genetic optimization algorithm to design a three-layer structure, consisting of a lossy layer sandwiched between a GST layer and a gain layer, to realize switching between self-dual SSs and unidirectional spectral singularities. We also investigate the underlying physical mechanism of the realized unidirectional spectral singularity. In Subsection 3.4 we design a singularity-enhanced active device with large modulation depth operating at the unidirectional spectral singularity. Finally, our conclusions are summarized in Section 4.

2. Theory

The optical properties of our proposed multilayer structure can be described by the transfer matrix $\mathbf{M}$ defined through [5,6]

$$\begin{bmatrix} E_R^- \\ E_R^+ \end{bmatrix} = \mathbf{M} \begin{bmatrix} E_L^+ \\ E_L^- \end{bmatrix} = \begin{bmatrix} M_{11} & M_{12} \\ M_{21} & M_{22} \end{bmatrix} \begin{bmatrix} E_L^+ \\ E_L^- \end{bmatrix}, \tag{1}$$

where E_L^+ and E_R^+ are the complex electric field amplitudes of the incoming waves at the left and right ports, respectively. Similarly, E_L^- and E_R^- are the complex electric field amplitudes of the outgoing waves from the left and right ports, respectively (Fig. 1). The transfer matrix for light propagating across the jth layer is given by [39]

$$\mathbf{M}_j = \begin{bmatrix} \cos(n_j k_0 d_j) & \frac{i}{n_j}\sin(n_j k_0 d_j) \\ i n_j \sin(n_j k_0 d_j) & \cos(n_j k_0 d_j) \end{bmatrix}, \tag{2}$$

where k_0 is the wavenumber in free space, d_j is the thickness of the jth layer, and n_j is the refractive index of the jth layer. The transfer matrix $\mathbf{M}$ of the entire multilayer structure is obtained by multiplying the transfer matrices of individual layers as follows

$$\mathbf{M} = \mathbf{A}^{-1}[\prod_{j=1}^{N} \mathbf{M}_j]\mathbf{A}, \tag{3}$$

where N is the number of layers, $\mathbf{A}$ is given by $\begin{bmatrix} 1 & 1 \\ 1 & -1 \end{bmatrix}$ and $\mathbf{A}^{-1}$ is its matrix inverse. The complex reflection coefficients $r_{L,R}$ and complex transmission coefficients $t_{L,R}$ for uniform plane waves normally incident from the left and from the right are obtained from the following equations [9]

$$\begin{aligned} r_L &= \frac{E_L^-}{E_L^+}\Big|_{E_R^+=0} = -\frac{M_{21}}{M_{22}}, \quad r_R = \frac{E_R^-}{E_R^+}\Big|_{E_L^+=0} = \frac{M_{12}}{M_{22}}, \\ t_L &= \frac{E_R^-}{E_L^+}\Big|_{E_R^+=0} = \frac{|\mathbf{M}|}{M_{22}}, \quad t_R = \frac{E_L^-}{E_R^+}\Big|_{E_L^+=0} = \frac{1}{M_{22}}. \end{aligned} \tag{4}$$

Note that the transmission coefficients for light incident from the left and from the right are equal due to reciprocity, that is, $t_L = t_R = t$. The transmission is $T = |t|^2$, while the reflection for light

Optics EXPRESS

incident from the left and from the right are $R_L = |r_L|^2$, and $R_R = |r_R|^2$, respectively. A *spectral singularity* corresponds to an optical system with purely outgoing radiation, that is, $E_L^+ = E_R^+ = 0$, $E_L^- \neq 0$, and $E_R^- \neq 0$, which implies that the system acts as a laser [9,15]. If these conditions are satisfied, we have

$$M_{22} = 0. \tag{5}$$

The SSs satisfying Eq. (5) are usually referred to as lasing singularities [40]. In contrast, *coherent perfect absorption*, as a time-reversed lasing process, corresponds to a system which completely absorbs the incident coherent radiation from both sides. That is, $E_L^+ \neq 0$, $E_R^+ \neq 0$, and $E_L^- = E_R^- = 0$. This happens when the following conditions are satisfied

$$M_{11} = 0, \quad E_R^+ = M_{21} E_L^+. \tag{6}$$

Singular points satisfying $M_{11} = 0$ are time-reversed SS and are also referred to as *absorbing singularities* [40]. A *self-dual spectral singularity* appears when the following conditions are satisfied

$$M_{11} = 0, \quad M_{22} = 0. \tag{7}$$

This corresponds to a SS which accompanies its time-reversed dual. An optical system which supports a self-dual SS at a given wavelength can act as not only a coherent perfect absorber with incident coherent radiation from both sides, but also as a laser without injected signals at the same wavelength. A self-dual SS is therefore referred to as a CPA-lasing singularity [16].

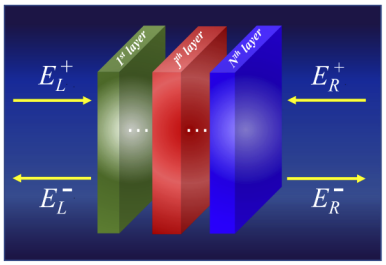

Fig. 1. Schematic of a multilayer optical structure.

Alternatively, the optical properties of our proposed system can also be described by the scattering matrix **S** defined by the following equation [5,6,41]

$$\begin{bmatrix} E_R^- \\ E_L^- \end{bmatrix} = \mathbf{S} \begin{bmatrix} E_L^+ \\ E_R^+ \end{bmatrix} = \begin{bmatrix} t & r_R \\ r_L & t \end{bmatrix} \begin{bmatrix} E_L^+ \\ E_R^+ \end{bmatrix}. \tag{8}$$

The eigenvalues of scattering matrix **S** are $\lambda_\pm = t \pm \sqrt{r_L r_R}$. Its eigenstates, which are $\Psi_\pm = (1, \pm\sqrt{\frac{r_L}{r_R}})^T$ for $r_R \neq 0$, or $\Psi_\pm = (\pm\sqrt{\frac{r_R}{r_L}}, 1)^T$ for $r_L \neq 0$, are not orthogonal. At *exceptional points* of the proposed optical system the eigenvalues and their corresponding eigenstates coalesce. The existence of EPs leads to unidirectional reflectionless propagation in either the left ($r_L = 0, r_R \neq 0$) or the right direction ($r_R = 0, r_L \neq 0$).

3. Results

In this section, we design non-*PT*-symmetric multilayer structures with phase-change material GST layers, to realize switching between singular points at the optical communication wavelength of $\lambda_0 = 1.55\mu$m. We use experimental data for the frequency-dependent dielectric constants of

Optics EXPRESS

all materials, including GST in its amorphous (aGST) and crystalline (cGST) phases [35]. The refractive indices of aGST and cGST at $\lambda_0 = 1.55\mu$m are $n_a = 4.4 + i0.098$ and $n_c = 7.1 + i0.78$, respectively [35]. In Figs. 2(a) and 2(b) we show the real and imaginary parts, respectively, of the refractive index of GST in its crystalline (cGST) and amorphous (aGST) phases as a function of wavelength.

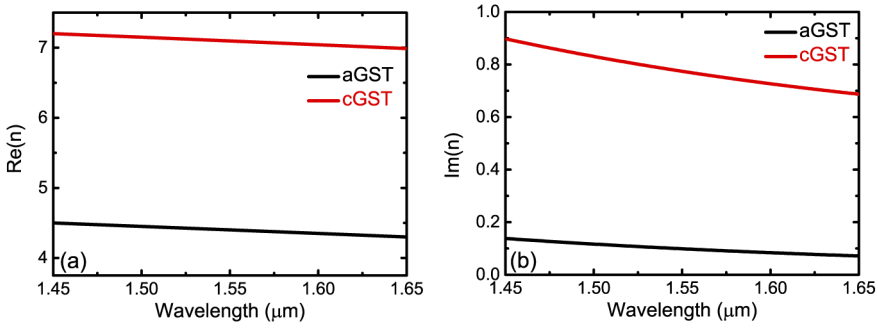

Fig. 2. (a), (b) Real and imaginary parts, respectively, of the refractive index of GST in its crystalline (cGST) and amorphous (aGST) phases as a function of wavelength.

3.1. Switching between absorbing singularities and exceptional points

To realize switching between absorbing singularities and EPs, and therefore between CPA and unidirectional reflectionlessness, we investigate a non-PT-symmetric two-layer structure composed of a GST layer and a lossy layer (Fig. 3). The lossy material has refractive index $n_2 = 2.02 + i\kappa$, corresponding to silicon dioxide doped with CdSe quantum dots [42–44]. This active absorbing material is tunable, since the imaginary part κ of the refractive index can be modified with an external control beam [42–44]. The experimentally achievable values of κ are in the range $0<\kappa<1$ with optical pump power densities of hundreds of W cm^{-2} [42–44]. Using the transfer matrix method (Section 2), we find that to achieve an absorbing singularity ($M_{11} = 0$) for normal incidence, when GST is in its crystalline phase, the following condition must be satisfied

$$e^{2ik_2d_2} = \frac{(n_2-1)[e^{2ik_cd_1}(n_c-n_2)(1+n_c)-(n_c+n_2)(1-n_c)]}{(n_2+1)[e^{2ik_cd_1}(n_c+n_2)(1+n_c)+(n_c-n_2)(1-n_c)]}. \tag{9}$$

Here, n_c is the refractive index of cGST, while k_c and k_2 are the wavenumbers in the cGST and lossy layers, respectively. In addition, if $M_{12} = 0$ and $M_{21} \neq 0$, we achieve unidirectional reflectionless propagation for plane waves normally incident from the right direction [Eq. (4)], and therefore an EP. Thus, to achieve an EP ($M_{12} = 0$) for normal incidence, when GST is in its amorphous phase, the following condition must be satisfied

$$e^{2ik_2d_2} = \frac{(n_2-1)[e^{2ik_ad_1}(n_2-n_a)(1-n_a)-(n_a+n_2)(1+n_a)]}{(n_2+1)[e^{2ik_ad_1}(n_2+n_a)(1-n_a)+(n_a-n_2)(1+n_a)]}, \tag{10}$$

where n_a is the refractive index of aGST, and k_a is the wavenumber in the aGST layer. Equation (9) is obtained by first analytically calculating the transfer matrix $\mathbf{M}$ using Eqs. (2) and (3), and then setting the matrix element M_{11} equal to zero ($M_{11} = 0$). Similarly, Eq. (10) is obtained by setting the matrix element $M_{12} = 0$ equal to zero ($M_{12} = 0$). Since the left hand sides of Eqs. (9) and (10) are the same and have magnitude less than one, to achieve a CPA to unidirectional reflectionlessness switch at the optical communication wavelength of $\lambda_0 = 1.55\mu$m, the right hand sides of Eqs. (9) and (10) must be equal and have magnitude less than one. We therefore choose the layer thickness d_1 (Fig. 3), as well as the imaginary part κ of the refractive index of

Optics EXPRESS

the tunable absorbing material, to make the right hand sides of Eqs. (9) and (10) equal and with magnitude less than one. Once we find d_1 and κ, we can use either Eq. (9) or Eq. (10) to find the thickness d_2 (Fig. 3). Using this approach, we find that for $d_1 = 266.4$ nm, $d_2 = 1728$ nm, and $\kappa = 0.051$ at $\lambda_0 = 1.55\mu$m, M_{11} is almost zero when GST is in its crystalline phase, and the reflection for waves incident from the right direction is almost zero as well when GST is in its amorphous phase. Thus, switching between absorbing singularities and EPs can be achieved in this two-layer structure by switching GST between its crystalline and amorphous phases.

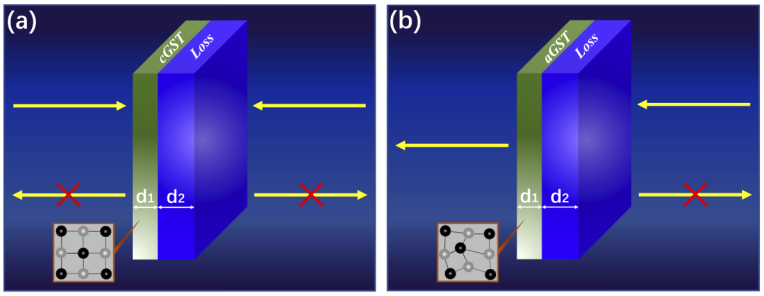

Fig. 3. Schematic of a non-*PT*-symmetric two-layer structure composed of a GST layer and a lossy layer for switching between absorbing singularities and EPs. The structure is designed to support (a) CPA at absorbing singularities with GST in its crystalline phase, and (b) unidirectional reflectionless propagation at EPs with GST in its amorphous phase.

To characterize light scattering by the proposed structure at absorbing singularities, we define a coefficient Θ as the ratio of the total intensity of outgoing waves to the total intensity of incoming waves [15,29]

$$\Theta = \frac{|E_R^-|^2 + |E_L^-|^2}{|E_R^+|^2 + |E_L^+|^2} = \frac{(|1 + \zeta M_{12}|^2) + |\zeta - M_{21}|^2}{(1 + |\zeta|^2)|M_{22}|^2}. \tag{11}$$

Here $\zeta = \frac{E_R^+}{E_L^+}$ is the ratio of the complex electric field amplitudes of the two normally incident incoming waves. Figure 4(a) shows Θ as a function of wavelength for the structure of Fig. 3(a) with GST in its crystalline phase (cGST). The ratio of the amplitudes of the incoming waves is chosen to be equal to M_{21} [Eq. (1)] at $\lambda_0 = 1.55\mu$m, i.e. $\frac{E_R^+}{E_L^+} = M_{21}\big|_{\lambda_0 = 1.55\mu m}$ [Eq. (6)]. The vanishing of Θ at $\lambda_0 = 1.55\mu$m is the signature of CPA at the absorbing singularity. Figure 4(b) shows the reflection spectra for the structure of Fig. 3(b) with GST in its amorphous phase (aGST) calculated for normally incident waves from both the left and right directions. These results confirm that this structure is unidirectional reflectionless due to the existence of an EP at $\lambda_0 = 1.55\mu$m, since the reflection in the right direction is almost zero, while the reflection in the left direction is nonzero. Thus, Figs. 4(a) and 4(b) verify that for the structure of Fig. 3 switching between absorbing singularities and EPs can be realized at the optical communication wavelength of $\lambda_0 = 1.55\mu$m by switching the phase-change material GST between its crystalline and amorphous phases.

3.2. Switching between spectral singularities and exceptional points

In this subsection, to realize switching between SSs and EPs, we investigate a non-*PT*-symmetric three-layer structure composed of a lossless dielectric layer sandwiched between a GST layer and a gain layer (Fig. 5). In contrast to EPs and absorbing singularities, SSs can only occur in the presence of gain [9,45]. The gain material we choose here has refractive index $n_3 = 3.44 - i\chi$, corresponding to InGaAsP with InAs quantum dots [46,47]. The real part of the refractive index of this gain material in the infrared is weakly dependent on the wavelength, while the imaginary

Optics EXPRESS

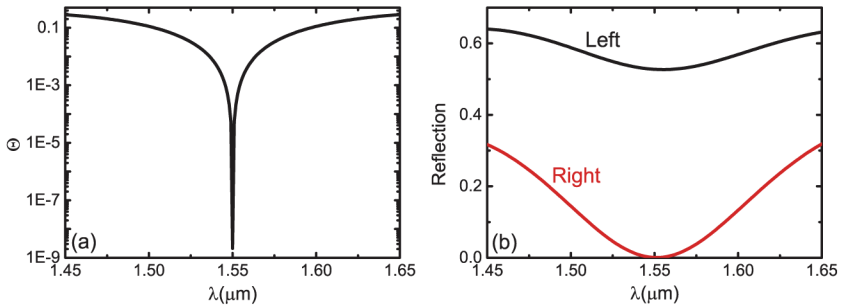

Fig. 4. Θ [Eq. (11)] as a function of wavelength for the structure of Fig. 3(a) with GST in its crystalline phase (cGST) calculated for normally incident coherent plane waves. Results are shown for $d_1 = 266.4$ nm, $d_2 = 1728$ nm, and $\kappa = 0.051$. The lossy material is silicon dioxide doped with CdSe quantum dots ($n_2 = 2.02 + i0.051$). (b) Reflection spectra for the structure of Fig. 3(b) with GST in its amorphous phase (aGST) calculated for normally incident waves from both the left and right directions. All other parameters are as in Fig. 4(a).

part χ can be controlled with an external beam [46,47]. The lossless dielectric is epitaxial TiO_2 (rutile) with refractive index $n_2 = 2.53$ at $\lambda_0 = 1.55\mu$m [48]. Using the transfer matrix method as described in Section 2, we optimize the thicknesses of all three layers, d_1, d_2 and d_3, as well as the imaginary part χ of the refractive index of the gain material (Fig. 5), to simultaneously make the amplitudes of the transfer matrix element M_{22}, when GST is in its crystalline phase, and of the reflection coefficient for plane waves normally incident from the right r_R, when GST is in its amorphous phase, as close to zero as possible at $\lambda_0 = 1.55\mu$m. The corresponding fitness function used in the optimization is therefore chosen to be

$$F(d_1, d_2, d_3, \chi) = |M_{22}|\big|_{cGST} + |r_R|\big|_{aGST}. \tag{12}$$

Since the transfer matrix method (Section 2) for the structure of Fig. 5 is computationally very efficient, we are able to use an exhaustive search in the design parameter space (d_1, d_2, d_3 and χ) to optimize the structure. Using this approach, we find that for $d_1 = 110.6$ nm, $d_2 = 97.7$ nm, $d_3 = 1145$ nm, and $\chi = 0.09$, M_{22} is almost zero, when GST is in its crystalline phase, and the reflection in the right direction is also almost zero, when GST is in its amorphous phase at $\lambda_0 = 1.55\mu$m. We note that there exist other points in the parameter space considered (d_1, d_2, d_3 and χ) that can also satisfy these constraints.

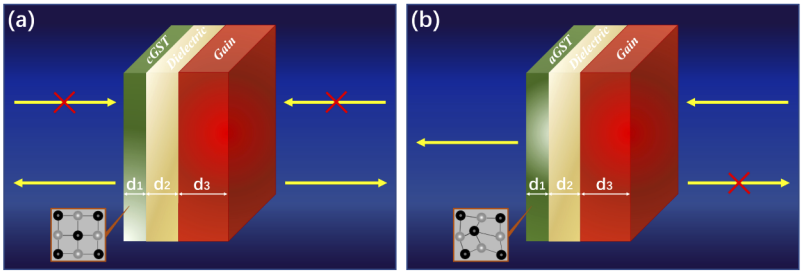

Fig. 5. Schematic of a non-*PT*-symmetric three-layer structure composed of a lossless dielectric layer sandwiched between a GST layer and a gain layer for switching between SSs and EPs. The structure is designed to support (a) lasing response at SSs with GST in its crystalline phase and (b) unidirectional reflectionless propagation at EPs with GST in its amorphous phase.

Optics EXPRESS

Figures 6(a), 6(b) and 6(c) show the transmission and reflection spectra for the structure of Fig. 5(a) with GST in its crystalline phase (cGST). We observe a lasing response when the wavelength of the incident light becomes $\lambda_0 = 1.55\mu$m. Greatly enhanced transmission and reflection with ultra-narrow linewidths are simultaneously achieved, which reveals the existence of a SS (M_{22}=0) in our optimized structure at $\lambda_0 = 1.55\mu$m. Figure 6(d) shows the reflection spectra for the structure of Fig. 5(b) with GST in its amorphous phase (aGST) calculated for normally incident waves from the left and right directions. These results also confirm that the optimized structure of Fig. 5(b) with aGST is unidirectional reflectionless at $\lambda_0 = 1.55\mu$m, since the reflection in the right direction is almost zero, while the reflection in the left direction is nonzero. Thus, we conclude that for the optimized structure of Fig. 5 switching between SSs and EPs can be realized at the optical communication wavelength by switching GST between its crystalline and amorphous phases. It is worth noting that the presence of the middle lossless dielectric layer is critical to achieve such switching between SSs and EPs. We found that a two-layer structure without this middle layer cannot achieve the same functionality. The middle dielectric layer is required in order to achieve destructive interference between reflected waves, which leads to zero reflection for waves incident from the right, and therefore to an exceptional point for GST in its amorphous phase.

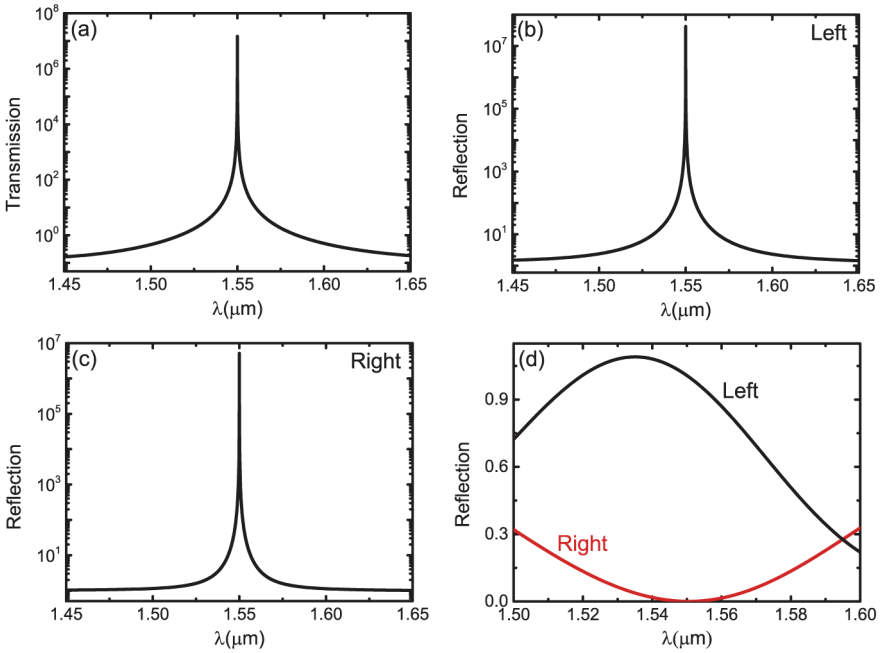

Fig. 6. (a) Transmission spectra for the optimized structure of Fig. 5(a) with GST in its crystalline phase (cGST) calculated for normal incidence. Results are shown for $d_1 = 110.6$ nm, $d_2 = 97.7$ nm, $d_3 = 1145$ nm, and $\chi = 0.09$. The lossless dielectric material is epitaxial TiO_2 (rutile) with refractive index $n_2 = 2.53$. The gain material is InGaAsP with InAs quantum dots ($n_3 = 3.44 - i0.09$). (b) and (c) Reflection spectra for the optimized structure of Fig. 5(a) with GST in its crystalline phase (cGST), when the light is normally incident from the left and right, respectively. All other parameters are as in Fig. 6(a). (d) Reflection spectra for the optimized structure of Fig. 5(b) with GST in its amorphous phase (aGST) calculated for normally incident waves from the left and right directions. All other parameters are as in Fig. 6(a).

Optics EXPRESS

3.3. Switching between self-dual spectral singularities and unidirectional spectral singularities

As we saw in the previous sections, to realize switching between CPA at absorbing singularities and unidirectional reflectionlessness at EPs, we use a structure which includes a lossy layer (Subsection 3.1). In addition, to realize switching between lasing at SSs and unidirectional reflectionlessness at EPs, we use a structure which includes a gain layer (Subsection 3.2). In this subsection, to realize switching between self-dual SSs and unidirectional spectral singularities, we consider a non-PT-symmetric three-layer structure composed of a lossy layer sandwiched between a GST layer and a gain layer (Fig. 7). The active absorbing material in the lossy layer is silicon dioxide doped with CdSe quantum dots, while the active gain material is InGaAsP with InAs quantum dots. In the optimization procedure we use a genetic algorithm which applies the concepts of evolution and natural selection [49,50]. More specifically, we use the transfer matrix method coupled with the genetic algorithm to optimize the thicknesses of all three layers, d_1, d_2, d_3 (Fig. 7), as well as the imaginary parts κ and χ of the refractive indices of the absorbing and gain materials, respectively, to simultaneously make the amplitudes of the transfer matrix elements M_{11} and M_{22}, when GST is in its amorphous phase, and of the reflection coefficient for plane waves normally incident from the left r_L, when GST is in its crystalline phase, as close to zero as possible at $\lambda_0 = 1.55\mu$m. The corresponding fitness function used in the optimization is therefore chosen to be

$$F(d_1, d_2, d_3, \kappa, \chi) = (|M_{11}| + |M_{22}|)\big|_{aGST} + |r_L|\big|_{cGST}. \tag{13}$$

In the genetic algorithm, the number of individuals in each population and the maximum number of generations are set equal to 50 and 10000, respectively. Using this approach, we find that for $d_1 = 1149.7$ nm, $d_2 = 352.8$ nm, $d_3 = 1365.9$ nm, $\kappa = 0.405$, and $\chi = 0.247$, the transfer matrix elements M_{11} and M_{22}, when GST is in its amorphous phase, and the reflection coefficient for plane waves normally incident from the left r_L, when GST is in its crystalline phase, are almost zero at $\lambda_0 = 1.55\mu$m.

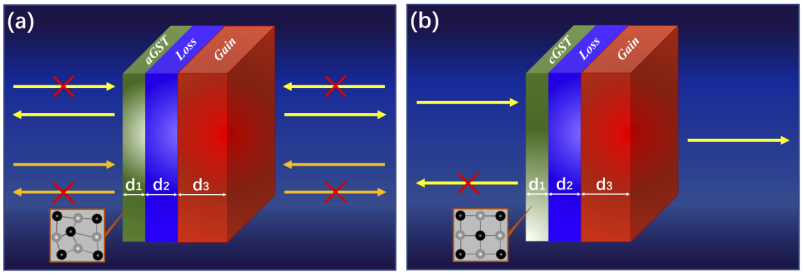

Fig. 7. Schematic of a non-PT-symmetric three-layer structure composed of a lossy layer sandwiched between a GST layer and a gain layer for switching between self-dual SSs and unidirectional spectral singularities. The structure is designed to support (a) CPA-lasing at self-dual SSs with GST in its amorphous phase, and (b) left reflectionless-right lasing at unidirectional spectral singularities with GST in its crystalline phase.

Figure 8(a) shows Θ [Eq. (11)] as a function of wavelength for the structure of Fig. 7(a) with GST in its amorphous phase (aGST) for normally incident coherent plane waves with the ratio of the amplitudes of the incoming waves set equal to $\frac{E_R^+}{E_L^+} = M_{21}\big|_{\lambda_0=1.55\mu m}$ [Eq. (6)]. We observe that Θ vanishes for the optimized structure of Fig. 7(a) at $\lambda_0 = 1.55\mu$m. Figures 8(b), 8(c) and 8(d) show the transmission and reflection spectra as a function of wavelength for the optimized structure of Fig. 7(a) with aGST. We observe that the reflection and transmission are greatly enhanced for $\lambda_0 = 1.55\mu$m. The vanishing of Θ [Fig. 8(a)], which is the signature of

Optics EXPRESS

coherent perfect absorption, in combination with the greatly enhanced transmission and reflection [Figs. 8(b), 8(c), 8(d)], which is a signature of a lasing response, provide convincing evidence of the existence of a self-dual SS in our optimized structure with aGST at $\lambda_0 = 1.55\mu$m. Such a system is a CPA-laser and can act either as a CPA or as a laser at $\lambda_0 = 1.55\mu$m.

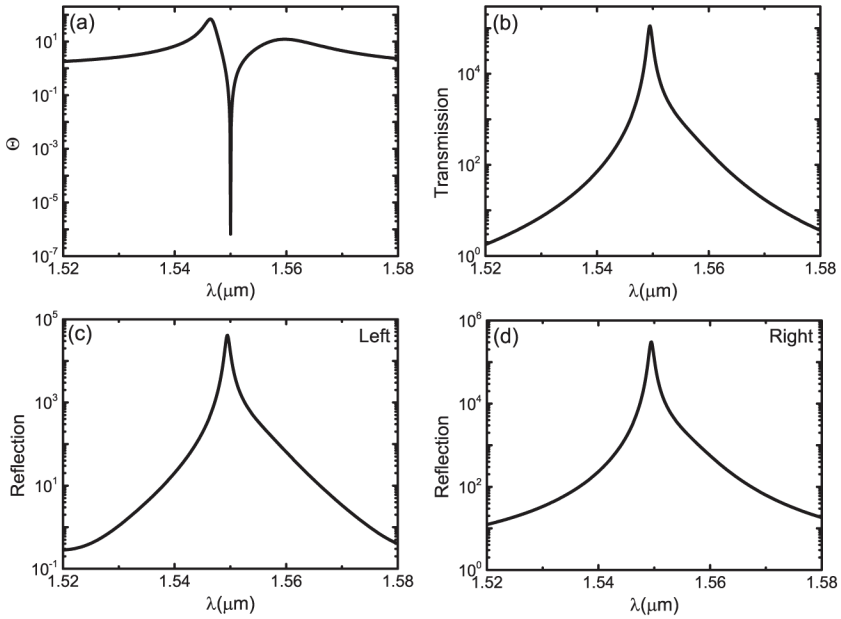

Fig. 8. (a) Θ [Eq. (11)] as a function of wavelength for the optimized structure of Fig. 7(a) with GST in its amorphous phase (aGST) calculated for normally incident coherent plane waves. Results are shown for $d_1 = 1149.7$ nm, $d_2 = 352.8$ nm, $d_3 = 1365.9$ nm, $\kappa = 0.405$, and $\chi = 0.247$. The lossy material is silicon dioxide doped with CdSe quantum dots ($n_2 = 2.02 + i0.405$). The gain material is InGaAsP with InAs quantum dots ($n_3 = 3.44 - i0.247$). (b) Transmission spectra for the optimized structure of Fig. 7(a) with aGST calculated for normal incidence. All other parameters are as in Fig. 8(a). (c) and (d) Reflection spectra for the optimized structure of Fig. 7(a) with aGST calculated for normally incident waves from the left and right directions, respectively. All other parameters are as in Fig. 8(a).

Figure 9(a) shows the reflection spectra for the optimized structure of Fig. 7(b) with GST in its crystalline phase (cGST) calculated for normally incident waves from both the left and right directions. It is interesting to note that at $\lambda_0 = 1.55\mu$m the reflection from the left (red) is close to zero, while the reflection from the right (black) tends to infinity. In other words, the optimized non-PT-symmetric structure with cGST simultaneously supports unidirectional reflectionlessness for incidence from the left, as well as a unidirectional lasing mode in the right. This exotic phenomenon has also been observed in PT-symmetric coupled cavity systems [21]. In these systems, such a phenomenon is obtained for $M_{12}(\lambda_0) \to \infty$, $M_{21}(\lambda_0) \to 0$, and $M_{22}(\lambda_0) \neq 0$ [21]. Figure 9(b) shows the amplitude of the transfer matrix elements $|M_{21}|$, $|M_{12}|$, and $|M_{22}|$ as a function of wavelength for the optimized structure of Fig. 7(b) with cGST. We observe that, in contrast to the coupled cavity systems [21], the simultaneous left reflectionless and right lasing in our case requires

$$M_{12}(\lambda_0) \neq 0, \quad M_{21}(\lambda_0) \to 0, \quad M_{22}(\lambda_0) \to 0. \tag{14}$$

Optics EXPRESS

First, $M_{12}(\lambda_0) \neq 0$ and $M_{22}(\lambda_0) \to 0$ [Fig. 9(b)] leads to diverging reflection from the right side ($\left|\frac{M_{12}(\lambda_0)}{M_{22}(\lambda_0)}\right|^2$) [Fig. 9(a)]. Second, $M_{21}(\lambda_0)$ approaching zero faster than $M_{22}(\lambda_0)$ [Fig. 9(b)] results in vanishing reflection from the left side ($\left|\frac{M_{21}(\lambda_0)}{M_{22}(\lambda_0)}\right|^2$) [Fig. 9(a)]. Thus, the simultaneous left reflectionless and right lasing in our structure emerges from the coincidence of two singularities at $\lambda_0 = 1.55\mu$m. In general, unidirectional reflectionlessness ($r_L \to 0$ and $r_R \neq 0$) is the signature of the existence of an EP associated with the coalescence of the eigenvalues $\lambda_\pm = t \pm \sqrt{r_L r_R}$ and their corresponding eigenvectors $\Psi_\pm = (1, \pm\sqrt{\frac{r_L}{r_R}})^T$. However, in the case of simultaneous left unidirectional reflectionless and right unidirectional lasing mode ($r_L \to 0$ and $r_R \to \infty$), as for the structure of Fig. 7(b) with cGST at $\lambda_0 = 1.55\mu$m, the system exhibits a unidirectional reflectionless singularity [21]. Note that the pseudounitary conservation relation $\sqrt{R_L R_R} = |T - 1|$ [5] still holds at this point. We conclude that for the optimized structure of Fig. 7 switching between self-dual SSs and unidirectional spectral singularities can be realized at the optical communication wavelength by switching the phase-change material GST between its amorphous and crystalline phases.

The extremely sharp line shape of the reflection from the left side [Fig. 9(a)] reveals that the underlying physical mechanism for the formation of simultaneous left unidirectional reflectionless and right unidirectional lasing mode is a strong resonance. This strong resonance results in light being trapped in the structure for a long period [51]. In Figs. 9(c) and 9(d), we observe that the phases of the reflection coefficients for the optimized structure of Fig. 7(b) with GST in its crystalline phase undergo abrupt jumps at $\lambda_0 = 1.55\mu$m when the light is incident from the left and right directions, respectively. The corresponding group delay experienced by the trapped light is given by $\tau_g = \frac{d\Phi(\lambda)}{d\lambda}$, where Φ is the phase of the transmission or reflection coefficient [51], and is therefore very large at $\lambda_0 = 1.55\mu$m. Thus, light reflected from the left side is trapped in the absorbing region for an extremely long period and is attenuated, while light reflected from the right side is strongly confined in the gain region and is amplified [21]. The simultaneous left reflectionless and right lasing phenomenon can also be observed in the electric field distributions for the optimized structure of Fig. 7(b) with cGST [Figs. 9(e) and 9(f)]. When the plane wave is normally incident from the left, there is hardly any reflection, as seen in Fig. 9(e) and its inset. When the plane wave is normally incident from the right, the reflected wave is enhanced by three orders of magnitude [Fig. 9(f)]. In addition, we observe large resonant enhancement of the electric field inside the loss and gain layers, when plane waves are normally incident from the left or right directions [Figs. 9(e) and 9(f)]. Note that the two field profiles in Figs. 9(e) and 9(f) are very similar except that the resonant field enhancement is much larger for waves normally incident from the right [Fig. 9(f)].

3.4. Design of extremely sensitive active devices at unidirectional spectral singularities

Figure 9(a) shows that the optimized structure of Fig. 7(b) with cGST is reflectionless for normally incident waves from the left direction (red line) in an ultra-narrow wavelength range with ~ 0.09 nm bandwidth. Figure 9(e) also shows that a large field enhancement is induced inside the middle lossy layer filled with the active absorbing material. These features provide an opportunity to design an extremely sensitive active device at the unidirectional spectral singularity. To characterize the sensitivity of the optimized structure of Fig. 7(b), we define the *figure of merit* (*FOM*) as the absolute value of the derivative of the reflection from the left R_L with respect to the imaginary part κ of the refractive index of the active absorbing material in the middle layer

$$FOM = \left|\frac{dR_L}{d\kappa}\right|, \tag{15}$$

Optics EXPRESS

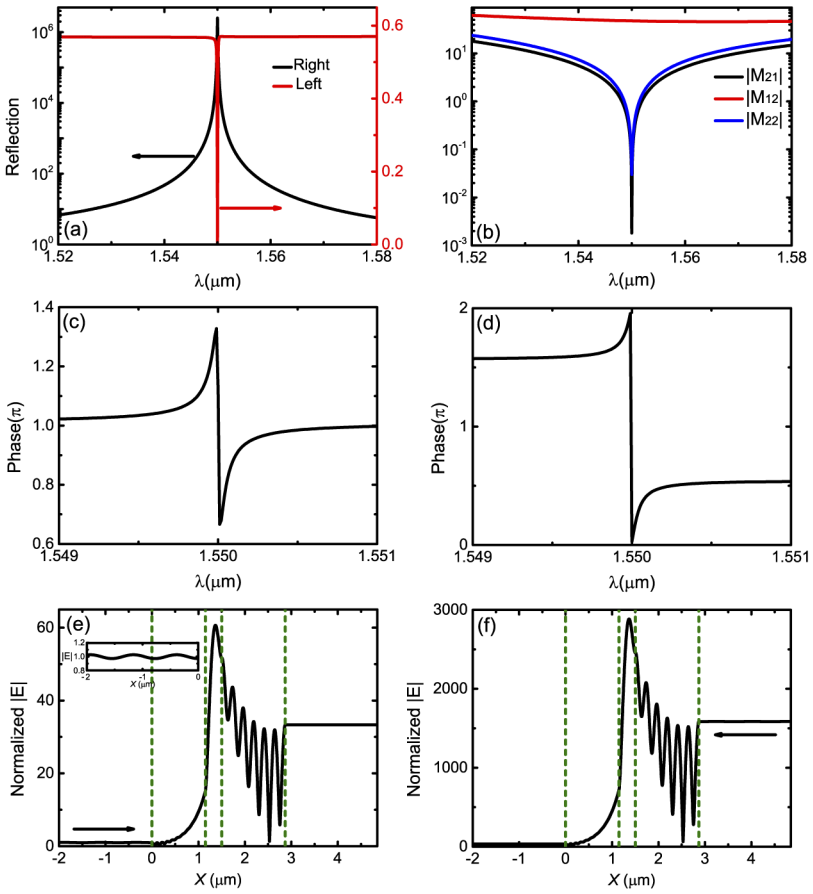

Fig. 9. (a) Reflection spectra for the optimized structure of Fig. 7(b) with GST in its crystalline phase (cGST) calculated for normally incident waves from both the left and right directions. All other parameters are as in Fig. 8(a). (b) Amplitude of the transfer matrix elements $|M_{21}|$, $|M_{12}|$, and $|M_{22}|$ as a function of wavelength for the optimized structure of Fig. 7(b) with cGST. All other parameters are as in Fig. 8(a). (c) and (d) Phase spectra of the reflection coefficients for uniform plane waves normally incident from the left (r_L) and from the right (r_R) directions for the structure of Fig. 7(b) with cGST. All other parameters are as in Fig. 8(a). (e) and (f) Profile of the electric field amplitude, normalized with respect to the field amplitude of the incident plane wave, in the optimized structure of Fig. 7(b) with cGST at $\lambda_0 = 1.55\mu$m, when the light is normally incident from the left and right, respectively. The vertical dashed lines indicate the boundaries between different layers. The inset in Fig. 9(e) shows the normalized field profile for $-2\mu\text{m} \le X \le 0\mu$m, when the light is normally incident from the left. All other parameters are as in Fig. 8(a).

Optics EXPRESS

where $R_L = |r_L|^2$. The *FOM* can be calculated using the following finite-difference approximation $\frac{dR_L}{d\kappa} \simeq \frac{R_L(\kappa+\Delta\kappa)-R_L(\kappa-\Delta\kappa)}{2\Delta\kappa}$. In our calculations, we use $\Delta\kappa = 10^{-4} << \kappa$ [50]. Figure 10(a) shows the calculated *FOM* as a function of wavelength. The maximum value of the *FOM* is ~ 3250 at the unidirectional spectral singularity ($\lambda_0 = 1.55\mu$m), which is one order of magnitude larger than the *FOM* in plasmonic waveguide-cavity devices [52].

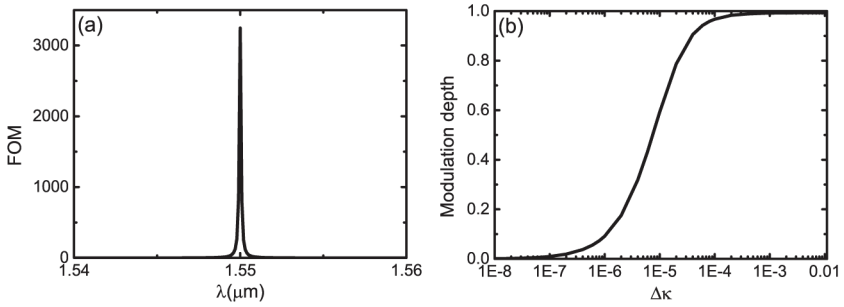

Fig. 10. (a) FOM [Eq. (15)] for the optimized structure of Fig. 7(b) with GST in its crystalline phase (cGST) as a function of wavelength. All other parameters are as in Fig. 8(a). (b) Modulation depth [Eq. (16)] for the optimized structure of Fig. 7(b) with cGST as a function of the variation $\Delta\kappa$ in the imaginary part of the refractive index of the active absorbing material filling the middle layer of the structure at $\lambda_0 = 1.55\mu$m. All other parameters are as in Fig. 8(a).

To characterize the singularity-enhanced performance of our optimized structure in Fig. 7(b), we further define the modulation depth [53]

$$M = \frac{I_{\text{on}} - I_{\text{off}}}{I_{\text{on}}}, \tag{16}$$

where I_{on} and I_{off} denote the intensity reflected by the optimized structure of Fig. 7(b) in the *on* ($\Delta\kappa \neq 0$) and *off* ($\Delta\kappa = 0$) states, respectively. Figure 10(b) shows the calculated modulation depth for the optimized structure of Fig. 7(b) with cGST as a function of the variation $\Delta\kappa$ in the imaginary part of the refractive index of the active absorbing material filling the middle layer of the structure at $\lambda_0 = 1.55\mu$m. We observe that a 3 dB (50%) modulation depth only requires a variation $\Delta\kappa \sim 8 \times 10^{-6}$ in the imaginary part of the refractive index of the active absorbing material, which is three orders of magnitude smaller than the one reported for plasmonic modulators [53]. In other words, large modulation depths can be obtained in such singularity-enhanced modulators with extremely small perturbations.

We note that our choice for the imaginary part of the refractive index of the active absorbing material ($\kappa = 0.405$) is within the range of experimentally achievable values [42–44]. In addition, the imaginary part of the refractive index of the gain material used in the optimized structure of Fig. 7 is 0.247, which corresponds to a gain coefficient of $g \approx 19683$ cm^{-1} [54]. Even though achieving the material gain required for our design is challenging, it could be realized with ultra-high-density quantum dot structures with injection current densities of tens of A cm^{-2} [55,56]. Finally, the layer thicknesses can be controlled by atomic layer deposition with an accuracy of 0.1 nm [57–59].

4. Conclusions

In this paper, we designed non-*PT*-symmetric multilayer structures for switching between different types of singular points using phase-change materials. We used the transfer matrix method to account for the behavior of the proposed structures. We first showed that absorbing singularities

Optics EXPRESS

can be switched to EPs in a two-layer structure consisting of a GST layer and a lossy layer, when GST transitions from its crystalline to its amorphous phase. We also showed that SSs can be switched to EPs in a three-layer structure consisting of a lossless dielectric layer sandwiched between a GST layer and a gain layer, when GST transitions from its crystalline to its amorphous phase. We then showed that self-dual SSs can be switched to unidirectional spectral singularities in a three-layer structure consisting of a lossy layer sandwiched between a GST layer and a gain layer, when GST transitions from its amorphous to its crystalline phase. We found that this structure supports a simultaneous left unidirectional reflectionless and right unidirectional lasing mode. In other words, a simultaneous zero reflection from the left side and infinite reflection from the right side is realized. The underlying physical mechanism of this exotic response is the coincidence of two different singularities and strong resonance-induced light trapping. Finally, we found that for such a structure the sensitivity of the reflection, when light is normally incident from the left, to variations of the refractive index of the active absorbing material filling the lossy layer is greatly enhanced at the unidirectional spectral singularity. Thus, the optimized structure operating at the unidirectional spectral singularity can be used as a modulator or switch.

As final remarks, the tolerance of the switching between absorbing singularities and exceptional points (Subsection 3.1) and between spectral singularities and exceptional points (Subsection 3.2) to parameter variations is quite good. For example, for switching between spectral singularities and exceptional points, for layer thickness variations of $d_1 = 110.6 \pm 5$ nm, $d_2 = 97.7 \pm 5$ nm, $d_3 = 1145 \pm 5$ nm, and for imaginary part of the refractive index of the gain material variations of $\chi = 0.09 \pm 0.01$, the resonance wavelength shift [Figs. 6(a), 6(b), 6(c)] is less than 0.02 μm, and the zero reflection wavelength shift [Fig. 6(d)] is less than 0.05 μm. In the case of switching between self-dual spectral singularities and unidirectional spectral singularities (Subsection 3.3), accuracy of 0.1 nm in the layer thicknesses is required which, as mentioned above, can be achieved by atomic layer deposition. In addition, as mentioned above, the phase transition in the phase-change material can be induced by thermal annealing, while the imaginary part of the refractive indices of the lossy and gain materials can be tuned via optical and electrical pumping, respectively. Thus, the properties of the proposed multilayer structures could be externally controlled via a combination of thermal annealing, optical pumping, and electrical pumping. We also note that, since the presence of gain and resonant features in the proposed devices lead to large field enhancement, it will be of interest to investigate the effect of nonlinearities on the devices. Our results could be potentially important for developing a new generation of compact singularity-enhanced switchable active optical devices. The concept of combining gain, loss, and phase-change materials for switching of singular points could also be applied to nanoplasmonic waveguide-cavity systems, which could lead to integrated optics implementations.

Funding. Natural Science Foundation of Hunan Province (2017JJ3375); National Natural Science Foundation of China (61605252).

Disclosures. The authors declare that there are no conflicts of interest related to this article.

References

1. N. Moiseyev, *Non-Hermitian Quantum Mechanics* (Cambridge University, 2011).
2. W. Heiss, "Exceptional points of non-Hermitian operators," J. Phys. A: Math. Gen. **37**(6), 2455–2464 (2004).
3. Z. Lin, H. Ramezani, T. Eichelkraut, T. Kottos, H. Cao, and D. N. Christodoulides, "Unidirectional invisibility induced by *PT*-symmetric periodic structures," Phys. Rev. Lett. **106**(21), 213901 (2011).
4. L. Feng, Y. L. Xu, W. S. Fegadolli, M. H. Lu, J. E. B. Oliveira, V. R. Almeida, Y. F. Chen, and A. Scherer, "Experimental demonstration of a unidirectional reflectionless parity-time metamaterial at optical frequencies," Nat. Mater. **12**(2), 108–113 (2013).
5. L. Ge, Y. D. Chong, and A. D. Stone, "Conservation relations and anisotropic transmission resonances in one-dimensional *PT*-symmetric photonic heterostructures," Phys. Rev. Lett. **85**(2), 023802 (2012).
6. Y. Huang, G. Veronis, and C. Min, "Unidirectional reflectionless propagation in plasmonic waveguide-cavity systems at exceptional points," Opt. Express **23**(23), 29882–29895 (2015).
7. X. Yin and X. Zhang, "Unidirectional light propagation at exceptional points," Nat. Mater. **12**(3), 175–177 (2013).

Optics EXPRESS

8. Y. Huang, Y. Shen, C. Min, S. Fan, and G. Veronis, "Unidirectional reflectionless light propagation at exceptional points," Nanophotonics **6**(5), 977–996 (2017).
9. A. Mostafazadeh, "Spectral singularities of complex scattering potentials and infinite reflection and transmission coefficients at real energies," Phys. Rev. Lett. **102**(22), 220402 (2009).
10. V. V. Konotop and D. A. Zezyulin, "Spectral singularities of odd-*PT*-symmetric potentials," Phys. Rev. A **99**(1), 013823 (2019).
11. A. Mostafazadeh, "Optical spectral singularities as threshold resonances," Phys. Rev. A **83**(4), 045801 (2011).
12. R. Aalipour, "Optical spectral singularities as zero-width resonance frequencies of a Fabry-Perot resonator," Phys. Rev. A **90**(1), 013820 (2014).
13. V. V. Konotop, E. Lakshtanov, and B. Vainberg, "Designing lasing and perfectly absorbing potentials," Phys. Rev. A **99**(4), 043838 (2019).
14. Y. D. Chong, L. Ge, H. Cao, and A. D. Stone, "Coherent perfect absorbers: time-reversed lasers," Phys. Rev. Lett. **105**(5), 053901 (2010).
15. S. Longhi, "*PT*-symmetric laser absorber," Phys. Rev. A **82**(3), 031801 (2010).
16. A. Mostafazadeh, "Self-dual spectral singularities and coherent perfect absorbing lasers without *PT*-symmetry," J. Phys. A: Math. Theor. **45**(44), 444024 (2012).
17. Y. D. Chong, L. Ge, and A. D. Stone, "*PT*-symmetry breaking and laser-absorber modes in optical scattering systems," Phys. Rev. Lett. **106**(9), 093902 (2011).
18. Z. Wong, Y. Xu, J. Kim, K. OBrien, Y. Wang, L. Feng, and X. Zhang, "Lasing and anti-lasing in a single cavity," Nat. Photonics **10**(12), 796–801 (2016).
19. M. Sakhdari, N. Estakhri, H. Bagci, and P. Chen, "Low-threshold lasing and coherent perfect absorption in generalized *PT*-symmetric optical structures," Phys. Rev. Appl. **10**(2), 024030 (2018).
20. W. Zhang, T. Wu, and X. Zhang, "Tailoring eigenmodes at spectral singularities in graphene-based *PT* systems," Sci. Rep. **7**(1), 11407 (2017).
21. H. Ramezani, H. Li, Y. Wang, and X. Zhang, "Unidirectional Spectral Singularities," Phys. Rev. Lett. **113**(26), 263905 (2014).
22. J. Doppler, A. Mailybaev, J. Bohm, U. Kuhl, A. Girschik, F. Libisch, T. Milburn, P Rabl, N. Moiseyev, and S. Rotter, "Dynamically encircling an exceptional point for asymmetric mode switching," Nature **537**(7618), 76–79 (2016).
23. S. Gangaraj and F. Monticone, "Topological waveguiding near an exceptional point: defect-immune, slow-light, and loss-immune propagation," Phys. Rev. Lett. **121**(9), 093901 (2018).
24. Y. Huang, C. Min, and G. Veronis, "Broadband near total light absorption in non-*PT*-symmetric waveguide-cavity systems," Opt. Express **24**(19), 22219–22231 (2016).
25. W. Chen, S. Ozdemir, G. Zhao, J. Wiersig, and L. Yang, "Exceptional points enhance sensing in an optical microcavity," Nature **548**(7666), 192–196 (2017).
26. H. Hodaei, A. Hassan, S. Wittek, H. Gracia, R. Ganainy, D. Christodoulides, and M. Khajavikhan, "Enhanced sensitivity at higher-order exceptional points," Nature **548**(7666), 187–191 (2017).
27. Y. Huang, Y. Shen, and G. Veronis, "Non-*PT*-symmetric two-layer cylindrical waveguide for exceptional-point-enhanced optical devices," Opt. Express **27**(26), 37494–37507 (2019).
28. M. Sakhdari, M. Farhat, and P. Chen, "*PT*-symmetric metasurfaces: wave manipulation and sensing using singular points," New J. Phys. **19**(6), 065002 (2017).
29. M. Farhat, M. Yang, Z. Ye, and P. Chen, "*PT*-symmetric absorber-laser enables electromagnetic sensors with unprecedented sensitivity," ACS Photonics **7**(8), 2080–2088 (2020).
30. K. Shportko, S. Kremers, M. Woda, D. Lencer, J. Robertson, and M. Wuttig, "Resonant bonding in crystalline phase-change materials," Nat. Mater. **7**(8), 653–658 (2008).
31. M. Rude, V. Mkhitaryan, A. E. Cetin, T. A. Miller, A. Carrilero, S. Wall, F. J. Abajo, H. Altug, and V. Pruneri, "Ultrafast and broadband tuning of resonant optical nanostructures using phase-change materials," Adv. Opt. Mater. **4**(7), 1060–1066 (2016).
32. D. Loke, T. H. Lee, W. J. Wang, L. P. Shi, R. Zhao, Y. C. Yeo, C. T. Chong, and S. R. Elliott, "Breaking the speed limits of phase-change memory," Science **336**(6088), 1566–1569 (2012).
33. M. Stegmaier, C. Rios, H. Bhaskaran, C. D. Wright, and W. H. P. Pernice, "Nonvolatile all-optical 1 × 2 switch for chipscale photonic networks," Adv. Opt. Mater. **5**(1), 1600346 (2017).
34. Y. Huang, Y. Shen, C. Min, and G. Veronis, "Switching of the direction of reflectionless light propagation at exceptional points in non-*PT*-symmetric structures using phase-change materials," Opt. Express **25**(22), 27283–27297 (2017).
35. J. Mu, Z. Han, S. Grillanda, A. Melloni, J. Michel, L. C. Kimerling, and A. Agarwal, "Towards ultra-subwavelength optical latches," Appl. Phys. Lett. **103**(4), 043115 (2013).
36. P. Hosseini, C. D. Wright, and H. Bhaskaran, "An optoelectronic framework enabled by low-dimensional phase-change films," Nature **511**(7508), 206–211 (2014).
37. M. A. Kats, R. Blanchard, P. Genevet, and F. Capasso, "Nanometre optical coatings based on strong interference effects in highly absorbing media," Nat. Mater. **12**(1), 20–24 (2013).
38. W. Zhang, R. Mazzarello, M. Wuttig, and E. Ma, "Designing crystallization in phase-change materials for universal memory and neuroinspired computing," Nat. Rev. Mater. **4**(3), 150–168 (2019).
39. L. Ge and F. Liang, "Contrasting eigenvalue and singular-value spectra for lasing and antilasing in a *PT*-symmetric periodic structure," Phys. Rev. A **95**(1), 013813 (2017).

Optics EXPRESS

40. C. Hang, G. Huang, and V. V. Konotop, "Tunable spectral singularities: coherent perfect absorber and laser in an atomic medium," New J. Phys. **18**(8), 085003 (2016).
41. Y. Li and C. Argyropoulos, "Exceptional points and spectral singularities in active epsilon-near-zero plasmonic waveguides," Phys. Rev. B **99**(7), 075413 (2019).
42. D. Pacifici, H. J. Lezec, and H. A. Atwater, "All-optical modulation by plasmonic excitation of CdSe quantum dots," Nat. Photonics **1**(7), 402–406 (2007).
43. D. Pacifici, H. Lezec, L. Sweatlock, C. Ruiter, V. Ferry, and H. Atwater, "All-optical plasmonic modulators and interconnects," in *Plasmonic nanoguides and circuits*, S. I. Bozhevolnyi, ed. (World Scientific, 2009).
44. C. Min and G. Veronis, "Absorption switches in metal-dielectric-metal plasmonic waveguides," Opt. Express **17**(13), 10757–10766 (2009).
45. M. Moccia, G. Castaldi, and A. Alu, "Harnessing spectral singularities in non-Hermitian cylindrical structures," IEEE Trans. Antennas Propag. **68**(3), 1704–1716 (2020).
46. V. E. Babicheva, I. V. Kulkova, R. Malureanu, K. Yvind, and A. V. Lavrinenko, "Plasmonic modulator based on gain-assisted metal-semiconductor-metal waveguide," Photonics and Nanostructures-Fundamentals Appl. **10**(4), 389–399 (2012).
47. M. Levinshtein, S. Rumyantsev, and M. Shur, *Handbook Series on Semiconductor Parameters*, (World Scientific, 1999).
48. S. Tanemura, L. Miao, P. Jin, K. Kaneko, A. Terai, and N. Nabatova-Gabain, "Optical properties of polycrystalline and epitaxial anatase and rutile TiO_2 thin films by rf magnetron sputtering," Appl. Surf. Sci. **212-213**, 654–660 (2003).
49. D. Goldberg, *Genetic Algorithms in Search, Optimization, and Machine Learning* (Addison Wesley, 1989).
50. Y. Huang, Z. Zhen, Y. Shen, C. Min, and G. Veronis, "Optimization of photonic nanojets generated by multilayer microcylinders with a genetic algorithm," Opt. Express **27**(2), 1310–1325 (2019).
51. Y. Huang, C. Min, P. Dastmalchi, and G. Veronis, "Slow-light enhanced subwavelength plasmonic waveguide refractive index sensors," Opt. Express **23**(11), 14922–14936 (2015).
52. H. Lu, X. Liu, D. Mao, and G. Wang, "Plasmonic nanosensor based on Fano resonance in waveguide-coupled resonators," Opt. Lett. **37**(18), 3780–3782 (2012).
53. W. Cai, J. S. White, and M. L. Brongersma, "Compact, high-Speed and power-efficient electrooptic plasmonic modulators," Nano Lett. **9**(12), 4403–4411 (2009).
54. M. P. Nezhad, K. Tetz, and Y. Fainman, "Gain assisted propagation of surface plasmon polaritons on planar metallic waveguides," Opt. Express **12**(17), 4072–4079 (2004).
55. N. Kirstaedter, O. G. Schmidt, N. N. Ledentsov, D. Bimberg, V. M. Ustinov, A. Y. Egorov, A. E. Zhukov, M. V. Maximov, P. S. Kopev, and Z. I. Alferov, "Gain and differential gain of single layer InAs/GaAs quantum dot injection lasers," Appl. Phys. Lett. **69**(9), 1226–1228 (1996).
56. K. Akahane, N. Yamamoto, and T. Kawanishi, "Fabrication of ultra-high-density InAs quantum dots using the strain-compensation technique," phys. stat. sol. (a) **208**(2), 425–428 (2011).
57. Y. Huang and L. Liu, "Recent progress in atomic layer deposition of molybdenum disulfide: a mini review," Sci. China Mater. **62**(7), 913–924 (2019).
58. Y. Zhou, H. Cheun, W. J. Potscavage, C. Hernandez, S. Kim, and B. Kippelen, "Inverted organic solar cells with ITO electrodes modified with an ultrathin Al_2O_3 buffer layer deposited by atomic layer deposition," J. Mater. Chem. **20**(29), 6189–6194 (2010).
59. M. Ritala, K. Kukli, A. Rahtu, P. I. Raisanen, M. Leskela, T. Sajavaara, and J. Keinonen, "Atomic layer deposition of oxide thin films with metal alkoxides as oxygen sources," Science **288**(5464), 319–321 (2000).